Suppressed Thermal Conductivity of Bi-layer Graphene with Vacancy-Initiated Linkages

Haifei Zhan[1,2], Yingyan Zhang[3], John M. Bell[1], and Yuantong Gu[1,*]

[1]*School of Chemistry, Physics and Mechanical Engineering, Queensland University of Technology, 2 George St, Brisbane QLD 4001, Australia*

[2]*Department of Material Science and NanoEngineering, Rice University, Houston, TX 77005, USA*

[3]*School of Computing, Engineering and Mathematics, University of Western Sydney, Locked Bag 1797, Sydney NSW 2751, Australia*

***Corresponding Author:** Prof. Yuantong Gu

Mailing Address: School of Chemistry, Physics and Mechanical Engineering,
Queensland University of Technology,
GPO Box 2434, Brisbane, QLD 4001, Australia

Telephones: +61-7-31381009 **Fax:** +61-7-31381469

E-mail: yuantong.gu@qut.edu.au

Abstract

Through larger-scale molecular dynamics simulations, we investigated the impacts from vacancy-initiated linkages on the thermal conductivity of bi-layer graphene sheets (of size $L \times W$=24.5 nm × 3.7 nm). Three different interlayer linkages, including divacancy bridging, "spiro" interstitial bridging and Frenkel pair defects, are considered. It is found that the presence of interlayer linkages induces a significant degradation in the thermal conductivity of the bi-layer graphene sheet. The degradation is strongly dependent on the interlayer linkage type, concentration and location. More importantly, the linkages that contain vacancies lead to more severe suppression of the thermal conductivity, in agreement with theoretical predictions that vacancies induce strong phonon scattering. Our finding provides useful guidelines for the application of multi-layer graphene sheets in practical thermal management.

Keywords: interlayer linkages, thermal conductivity, bi-layer graphene sheet, phonon scattering, molecular dynamics simulations

Introduction

Similarly to the monolayer graphene, bi-layer graphene has been reported to possess excellent mechanical, electrical, chemical and thermal properties. For example, the thermal conductivity of a bi-layer graphene has been measured as 2800 $Wm^{-1}K^{-1}$ at room temperature,[1] and its mobility has been reported as high as 40,000 $cm^2V^{-1}s^{-1}$ in air at room temperature on *h*-BN substrate.[2] The extraordinary properties of bi-layer graphene make it as a promising building block for nanoscale devices, composite materials and batteries,[3] such as flexible electrodes for touch screen displays,[4-5] microprocessors,[6] thermoelectric and photonic devices.[7] For the nanoscale devices, an

appropriate thermal conductivity (either low or high) of the material is a critical requirement for the thermal management purpose due to significantly increasing power densities in modern nanoscale devices.[8] For instance, some electronic devices demand efficient heat removal so as to maintain their operating performance and long-term reliability. For the thermoelectric devices, however, materials with suppressed thermal conductivity are required to ensure a high figure of merit. Recent years have witnessed an explosion in research on the thermal conductivity of advanced materials, especially the monolayer graphene. Researchers have reported that the thermal transport properties of graphene rely on a wide range of factors,[9-10] such as the geometry size,[11] axial strain,[12] functionalization,[13] and contact interfaces.[14]

The excellent thermal conductivity of graphene originates from the strongest covalent sp^2 bonds in nature. Therefore, the straightforward way to tailor the thermal transport of graphene is the modulation of sp^2 bonds. One popular method is chemical doping, such as N, B, and C isotopes,[15] which retain the sp^2 bonds but introduce weaker bonds (e.g., N-C, B-C) to the structure.[16] According to perturbation theory,[17] the strength of the phonon-point defect scattering Γ resulted from the dopant composition can be expressed by a summation of the mass-difference scattering $\Gamma_i^m = (1 - M_i / \bar{M})^2$ and ambiguous volume or bond-strength-difference scattering $\Gamma_i^b = \varepsilon[\gamma(1 - R_i / \bar{R})]^2$ as $\Gamma = \sum_i f_i(\Gamma_i^m + \Gamma_i^b)$, where f_i, M_i and R_i are the fractional concentration, mass and Pauling ionic radius of the ith substitutional atom, respectively. $\bar{M}$ and $\bar{R}$ are the average atomic mass and average radius, respectively. γ is the Gruneisen parameter (which is related to the anharmonicity of the lattice), and ε is the phenomenological parameter. Apparently, dopant atoms can exert a great influence to the phonon scattering mechanisms of the materials and their associated thermal properties.

In addition, based on the bond-order-length-strength correlation mechanism, Xie *et al*.[18] reported that the phonon scattering rate due to the change of force constant in two-dimensional materials is 3-10 folds larger than that due to missing mass and linkages, signifying that the vacancies exert crucial effects on the thermal transport properties of graphene. Consistently, monatomic vacancies and Stone-Thrower-Wales defects[19] are found to induce remarkable changes to the thermal transport properties of graphene. Moreover, the presence of sp^3 bonds in the monolayer graphene via functionalization, e.g., hydrogenation,[20] C_5H_{12}-functionalization[21] and fluorination[22] are also reported to exert significant impacts on its thermal conductivity.

Although numerous researches have been devoted to exploring effective avenues to tune the thermal conductivity of monolayer graphene, the investigations on bi-layer graphene are relatively lacking. Recent works reported that the inter-layer phonon coupling and scattering play a crucial role in determining the thermal conductivity of bi-layer graphene,[23] and the phonons can be effectively modulated by twisting the atomic planes.[24] Motivated by the suppression effects from vacancies and sp^3 bonds on the thermal conductivity of monolayer graphene, here we investigate how the thermal transport properties of a bi-layer graphene sheet (GS, of size $L\times W$=24.5 nm × 3.7 nm) can be tailored by different vacancy-initiated interlayer linkages. Experiments have confirmed that electron irradiation[25] and femto second-laser excitation[26] can create interwall bonds for graphite and pristine multiwall carbon nanotubes (MWCNTs). The signatures of sp^3-linked bilayer GS on adjacent GSs has also been evidenced by the quantum molecular dynamics calculations.[27] Researchers have also found that these interlayer/interwall linkages can enhance the mechanical properties of MWCNTs,[25] and bi-layer GS.[28-29]

Computational Methods

The impacts from different interlayer linkages on the thermal conductivity of bi-layer GS are explored via the reverse non-equilibrium molecular dynamics (RNEMD) simulations. All the simulations are performed by using the software package LAMMPS.[30] The essence of RNEMD is to generate a heat flux on the sample by exchanging the atomic velocities in different slabs.[31] After the stable state is achieved, the heat flux J (in unit of Watt) can be calculated by $J = 1/2tA\sum_{N}\frac{m}{2}(v_{hot}^2 - v_{cold}^2)$, where t is the time duration for the exchange, A is the cross-sectional area, N is the total number of exchanges, m is the atomic mass, v_{hot} and v_{cold} are the velocities of the hot and cold atoms that involved in the exchange, respectively. The thermal conductivity κ is calculated using the Fourier's law, $\kappa = -J/(\partial T/\partial x)$, where $\partial T/\partial x$ is the temperature gradient along the heat flux direction, which can be estimated from the resulting temperature profile of the sample.

Three different types of interlayer linkages are formed due to the presence of vacancy defects,[25, 32] including $V_2^1(\beta\beta)$ divacancy bridging (with two twofold coordinated C atoms surrounding each vacancy), "spiro" interstitial bridging (with a fourfold coordinated C atom inserted between the two graphene layers) and a Frenkel pair defect (a threefold coordinated C atoms sits below the vacancy in the upper layer). The atomic configurations of these interlayer linkages are illustrated in Figure 1 and denoted as L-A, L-B, and L-C for easy reference, respectively. The concentration of interlayer linkages is defined as the number of interlayer linkages divided by the total number of atoms in the pristine bi-layer GS. A bi-layer GS with a length of 24.5 nm and width of 3.7 nm was chosen. We note that different simulation domain sizes will influence the absolute value of the thermal conductivity.[21] Our discussions, however,

focus on the relative thermal conductivity of the bilayer graphene to avoid such influence. The atomic interactions are described by the widely used adaptive intermolecular reactive empirical bond order (AIREBO) potential.[33] Owing to the presence of sp^3 bonds, a small time step of 0.2 fs was used to ensure the stability of the simulation. After achieving the initial equilibrium configuration, the bi-layer GS was equilibrated using Nose-Hoover thermostat[34-35] under an ambient condition for 200 ps (i.e. temperature = 300 K and pressure = 1 atm). The system was then switched to the microcanonical ensemble for 1.2 ns. Periodic boundary conditions were applied in both lateral directions.

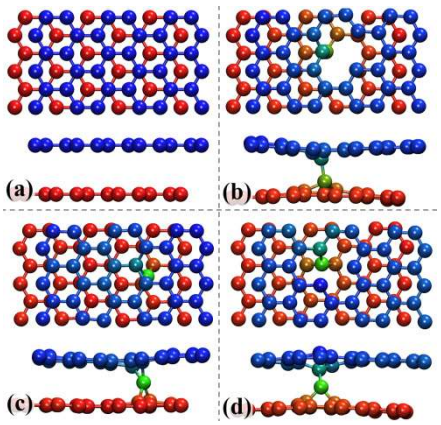

Figure 1. Atomic configurations of a bi-layer graphene model with and without linkages: (a) pristine; (b) L-A: $V_2^1(\beta\beta)$ divacancy bridging; (c) L-B: "spiro" interstitial bridging; and (d) L-C: Frenkel pair defect.

Results and Discussion

Randomly distributed interlayer linkages

First, we estimated the thermal conductivity for a pristine bi-layer GS, κ_p as a reference. The thermal conductivity of the pristine bi-layer GS is around 64.8 ± 3.8 W/mK by assuming a thickness of 0.67 nm (0.335nm for a monolayer GS), which is in good agreement with that obtained by other researchers.[36] It is worth noting that the

adoption of different thickness values and different atomic potentials would yield different thermal conductivity values. To avoid the thickness effect, we will emphasize on the relative thermal conductivity as defined by κ / κ_p.

Figure 2a clearly shows that the presence of the interlayer linkages leads to a large reduction in the thermal conductivity, in agreement with the finding for the bi-layer GS with interlayer sp^3 bonds.[36] For instance, 0.52% of $V_2^1(\beta\beta)$ divacancy bridgings (L-A) are found to reduce the thermal conductivity of the bilayer GS by 60%. Among the three types of interlayer linkages, the "spiro" interstitial bridgings (L-B) lead to the least reduction, followed by Frenkel pair defect (L-C) and divacancy bridgings (L-A). More specifically, κ exhibits a steep reduction in the low concentration level (<0.5%). Thereafter, κ decreases gradually and approaches to a constant value. For the bi-layer GS with 1.39% concentration of $V_2^1(\beta\beta)$ divacancy bridging, a significant reduction of κ as high as 80% is observed. We note that Liu *et al.*[37] reported that the covalent cross-linkers could enhance the thermal conductance of graphene. Such contradictory observations originate from the difference of thermal conductivity and models being investigated, i.e., they studied the cross-plane thermal conductivity of two partially overlapped parallel graphene nanoribbon while we investigated the in-plane thermal conductivity of a bi-layer graphene GS here.

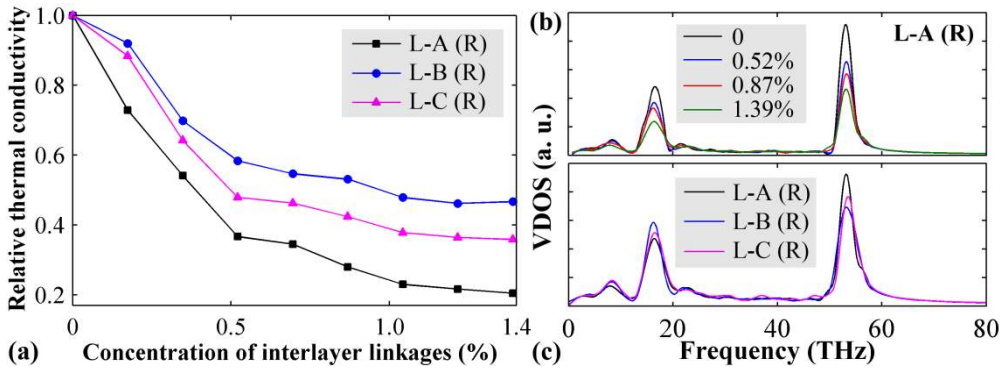

Figure 2. (a) Variation of the relative thermal conductivity with respect to the concentration of the randomly distributed (denoted as "R") interlayer linkages; (b) VDOS of the bi-layer GS with different concentration of $V_2^1(\beta\beta)$ divacancy bridgings; (c) Comparison of VDOS of the bi-layer GS with 1.39% concentration of different interlayer linkages.

To probe the underlying reasons for the κ reduction, we calculated the vibration density of states (VDOS) for the pristine and the defective bi-layer GS with different interlayer linkages. The VDOS is computed using the autocorrelation function of the atomic velocities.[38] As compared in Figure 2b, the presences of $V_2^1(\beta\beta)$ divacancy bridgings (L-A) have induced a significant reduction to the VDOS for both the in-plane (high-frequency) and out-of-plane (low-frequency) phonon modes, and the reduction increases with increasing linkage concentration. This observation explains the greatly suppressed κ when the interlayer linkages are introduced to the sample. In addition, as illustrated in Figure 2c, the impact on the in-plane and out-of-plane phonon modes varies with different interlayer linkages. For the "spiro" interstitial bridging (L-B in Figure 1c containing five sp^3 bonds but no vacancy), the presence of weaker sp^3 bonds (comparing with sp^2 bonds) is found to lead to the largest reduction in the amplitude of the in-plane phonon modes. On the other hand, the $V_2^1(\beta\beta)$ divacancy bridgings (L-A, which contains two vacancies but no sp^3 bonds in Figure 1b) are found to lead to the largest reduction in the amplitude of the out-of-plane phonon modes, but smallest reduction in the in-plane phonon modes. In conjugation with the relative κ presented in Figure 2a, it is suggested that the GS with stronger out-of-plane phonon modes intends to possess a higher thermal conductivity. Such observation is in agreement with the previous theoretical study that

the thermal conductivity of vacancy defective graphene is dominated by low-frequency acoustic phonons.[18]

More specifically, we notice that the two groups of results from the models containing vacancies (L-A and L-C) are also consistent with the recent theoretical predictions based on the bond-order-length-strength correlation mechanism.[39] Apart from the Umklapp phonon-phonon scattering ($\tau_{U,\lambda}^{-1}$) and the phonon-boundary scattering ($\tau_{B,\lambda}^{-1}$),[40] the vacancies can introduce another two phonon scattering mechanisms, including the missing mass and linkages (τ_V^{-1}), and the change of force constant k_z of bonds between the under-coordinated atoms adjacent to the vacancies (τ_A^{-1}).[18] For graphene, the phonon scattering induced by the under-coordinated atoms near the vacancies is derived as:[18]

$$\tau_A^{-1} = 4\pi z x \left\{ k_{z-1} / k_z - 1 \right\}^2 \frac{\omega^2 g(\omega)}{G} \quad (1)$$

where z is the coordination number (CN) and x is the density of single vacancy. k_{z-1} / k_z is the force constant ratio between the C atom around a single vacancy (CN=2) and a normal C atom (CN=3), which is estimated as 2.03. $g(\omega)$ is the phonon density of states, and G is the number of atoms in the crystal. From Eq. (1), it is evident that the bi-layer GS with more vacancies ($V_2^1(\beta\beta)$ divacancy bridgings) will induce severer phonon scattering, and thus lead to a lower thermal conductivity.

Longitudinal interlayer linkages pattern

Next, we assessed the influence from the locations of the interlayer linkages on the thermal conductivity of the bi-layer GS. Figure 3 shows the relative thermal conductivity as a function of the concentration of interlayer linkages when they are

aligned along the length direction of the sample (see inset of Figure 3). Similar as the findings in the previous section, the relative κ decreases monotonically with the increasing concentration of interlayer linkages, and the presence of $V_2^1(\beta\beta)$ divacancy bridgings (L-A) leads to the largest reduction. Particularly, the longitudinally aligned interlayer linkages are found to induce less reduction to the thermal conductivity when comparing with the randomly distributed interlayer linkages in Figure 2a.

More interestingly, the relative thermal conductivity almost decreases linearly with increasing interlayer linkage concentration, following the mixture rule in composites.[41] According to the mixture rule, for the structure with longitudinally aligned interlayer linkages, the effective thermal conductivity follows $\kappa_{eff} = (1-x)\kappa_p + x \cdot \kappa_l$, where κ_l denotes the thermal conductivity of the bi-layer GS with full coverage of interlayer linkages, and *x* is the density of the interlayer linkages. Though it is hard to define the full coverage of interlayer linkages (and also the corresponding thermal conductivity), Figure 3 shows that the results obtained from the sample with "spiro" interstitial bridgings (L-B) agree well with the linear fitting from the mixture rule. However, the effective thermal conductivity obtained for the other two interlayer linkages diverge from this linear relation.

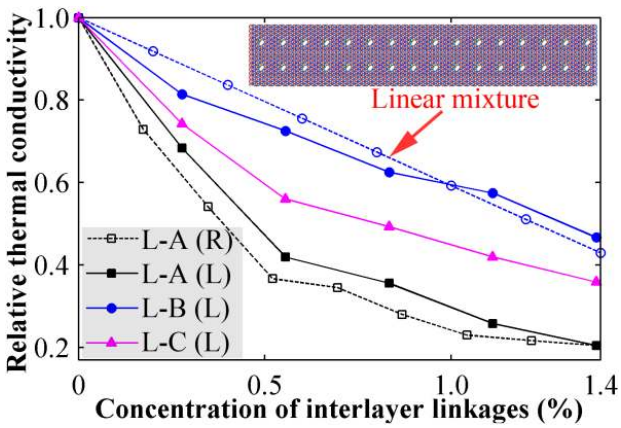

Figure 3. Relative thermal conductivity as a function of the longitudinally patterned (denoted as "L") interlayer linkages concentration. Inset shows a simulated model.

Transverse interlayer linkages pattern

We also examined the bi-layer GS with transversely aligned interlayer linkages (a representative model is shown in inset of Figure 4a). It is apparent from Figure 4a that the relative thermal conductivity decreases with increasing linkages' concentration, and a most significant impact is observed from the $V_2^1(\beta\beta)$ divacancy bridgings (L-A) followed by the Frenkel pair defect (L-C). Comparing the structures with random and longitudinally aligned interlayer linkages, the transversely patterned linkages are found to exert larger impacts on the thermal transport of the sample. Reconsidering the mixture rule,[41] when the linkages are transversely aligned, the effective thermal conductivity follow $\kappa_{eff} = \kappa_p \cdot \kappa_l / [(1-x)\kappa_l + x \cdot \kappa_p]$. However, as shown in Figure 4a for the bi-layer GS with "spiro" interstitial bridging (L-B), there are big discrepancies between the mixture rule and the MD results. These may be attributed to the following factors. The dominant origin is the interfacial phonon scattering at the interfaces between the pristine graphene and graphene with interlayer linkages. As illustrated in Figure 4b, the interface is found to result in a local temperature drop, indicating the existence of interfacial thermal resistance. Because of the local temperature drop, the temperature gradient $\partial T / \partial x$ in the calculation of κ is derived by fitting the two temperature values near the cold and hot regions (see the blue line in Figure 4b). From the VDOS in the pristine and modified regions (regions I and II highlighted in inset of Figure 4a), we found an obvious mismatch of the VDOS in Figure 4c, signifying the interfacial phonon scattering. Such interfacial phonon

scattering stems from the mismatch number of interface atoms or the mismatch structures, which cannot be captured in the mixture rule.

It is interesting to note that, unlike the GS with random and longitudinally aligned interlayer linkages, the relative thermal conductivity exhibits a U-shape profile due to the presence of transversely aligned linkages. Similar results have also been reported for the graphene with functional groups[21] and carbon isotopes.[42] The U-shape thermal conductivity is in agreement with the theoretical model for alloy semiconductors,[43] e.g., Si_xGe_{1-x}, $Al_xGa_{1-x}As$, which predicts the highest thermal conductivity for the material with either x=0 or x=1 and a fast decrease to a minimum as x deviates from 0. Besides the impacts from the pattern of interlayer linkages and interfacial phonon scattering, the different influence on the in-plane and out-of-plane phonon modes induced by the linkages, and also the competitions between different phonons' contributions are also responsible for the U-shape thermal conductivity. To identify those factors, further work is in progress.

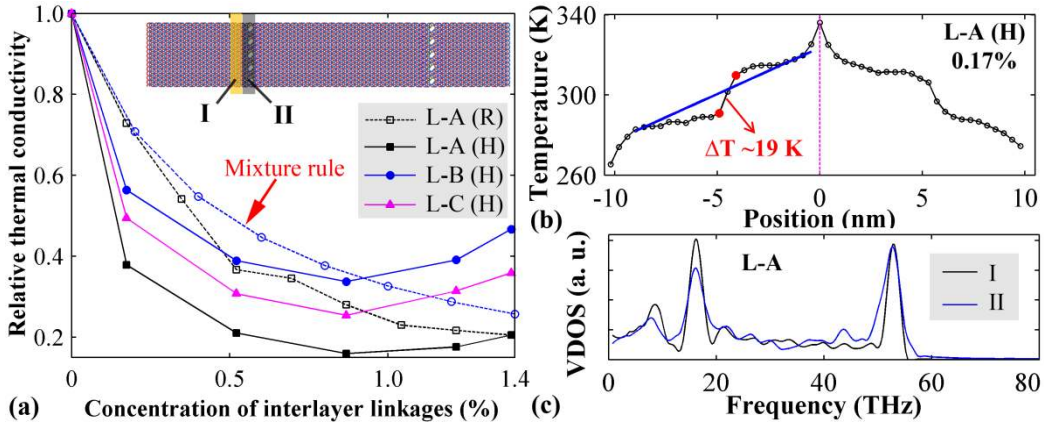

Figure 4. (a) Relative thermal conductivity as a function of the transversely patterned (denoted as "H") interlayer linkages concentration, inset shows a simulated model; (b) Temperature profile of the bi-layer GS with transversely patterned $V_2^1(\beta\beta)$ divacancy bridgings; (c) Comparison of the VDOS between the pristine bi-layer GS region (I) and defective region (II) with $V_2^1(\beta\beta)$ divacancy bridgings.

From the simulation results in Figures 2a, 3 and 4a, it is concluded that $V_2^1(\beta\beta)$ divacancy bridgings (L-A) lead to the largest reduction to κ while the "spiro" interstitial bridgings (L-B) has the least influence. In view of the fact that the L-A and L-C interlayer linkages contain two (none sp^3 bonds) and one vacancies (two sp^3 bonds), respectively, whereas the L-B linkage has five sp^3 bonds (but no vacancies), it is evident that the interlayer linkage with vacancies is able to cause larger reduction to the thermal conductivity than the one with sp^3 bonds. In other words, the vacancy is more efficient in degrading the thermal transport of the bi-layer GS than sp^3 bonds.

Conclusions

In summary, we performed intensive MD simulations to investigate the thermal conductivity of the bi-layer GS with different interlayer linkages, i.e., $V_2^1(\beta\beta)$ divacancy bridgings, "spiro" interstitial bridging and Frenkel pair defect. It is found that the thermal conductivity of the bi-layer GS can be effectively tailored through the introduction of different interlayer linkages, and the impacts from the interlayer linkages can be further modulated through their density and distribution. Up to 80% reduction in the thermal conductivity is achieved for the bilayer GS with 1.39% divacancy bridgings. We also found that the interlayer linkages with vacancies ($V_2^1(\beta\beta)$ divacancy bridgings and Frenkel pair defect) are more efficient in suppressing the thermal conductivity, in good agreement with the previous theoretical studies based on the bond-order-length-strength mechanism. It is believed that the present study can offer an important guideline for the design and application of bi-layer and multi-layer GS in nanoscale thermoelectric devices where suppressed thermal conductivity is essential.

Acknowledgment

Supports from the ARC Discovery Project (DP130102120) and the High Performance Computer resources provided by the Queensland University of Technology and Intersect Australia Ltd are gratefully acknowledged.

References

(1) Ghosh, S.; Bao, W.; Nika, D. L.; Subrina, S.; Pokatilov, E. P.; Lau, C. N.; Balandin, A. A., Dimensional Crossover of Thermal Transport in Few-Layer Graphene. *Nat. Mater.* **2010,** *9*, 555-558.
(2) Dean, C.; Young, A.; Meric, I.; Lee, C.; Wang, L.; Sorgenfrei, S.; Watanabe, K.; Taniguchi, T.; Kim, P.; Shepard, K., Boron Nitride Substrates for High-Quality Graphene Electronics. *Nat. Nanotechnol.* **2010,** *5*, 722-726.
(3) Zheng, H.; Zheng, J.-j.; He, L.; Zhao, X., Unique Configuration of a Nitrogen-Doped Graphene Nanoribbon: Potential Applications to Semiconductor and Hydrogen Fuel Cell. *J. Phys. Chem. C* **2014,** *118*, 24723-24729.
(4) Bae, S.; Kim, H.; Lee, Y.; Xu, X.; Park, J.-S.; Zheng, Y.; Balakrishnan, J.; Lei, T.; Kim, H. R.; Song, Y. I., Roll-to-Roll Production of 30-Inch Graphene Films for Transparent Electrodes. *Nat. Nanotechnol.* **2010,** *5*, 574-578.
(5) Lin, Y.; Jin, J.; Kusmartsevab, O.; Song, M., Preparation of Pristine Graphene Sheets and Large-Area/Ultrathin Graphene Films for High Conducting and Transparent Applications. *J. Phys. Chem. C* **2013,** *117*, 17237-17244.
(6) Shih, C.-J.; Vijayaraghavan, A.; Krishnan, R.; Sharma, R.; Han, J.-H.; Ham, M.-H.; Jin, Z.; Lin, S.; Paulus, G. L. C.; Reuel, N. F., et al., Bi- and Trilayer Graphene Solutions. *Nat Nano* **2011,** *6*, 439-445.
(7) McCann, E.; Koshino, M., The Electronic Properties of Bilayer Graphene. *Rep. Prog. Phys.* **2013,** *76*, 056503.
(8) Toberer, E.; Baranowski, L.; Dames, C., Advances in Thermal Conductivity. *Annu. Rev. Mater. Res.* **2012,** *42*, 179-209.
(9) Yang, N.; Xu, X.; Zhang, G.; Li, B., Thermal Transport in Nanostructures. *AIP Advances* **2012,** *2*, 041410.
(10) Liu, H. K.; Lin, Y.; Luo, S. N., Grain Boundary Energy and Grain Size Dependences of Thermal Conductivity of Polycrystalline Graphene. *J. Phys. Chem. C* **2014,** *118*, 24797-24802.
(11) Balandin, A. A.; Ghosh, S.; Bao, W.; Calizo, I.; Teweldebrhan, D.; Miao, F.; Lau, C. N., Superior Thermal Conductivity of Single-Layer Graphene. *Nano Lett.* **2008,** *8*, 902-907.
(12) Pei Shan Emmeline, Y.; Kian Ping, L.; Chee Kwan, G., Strain Dependence of the Heat Transport Properties of Graphene Nanoribbons. *Nanotechnology* **2012,** *23*, 495702.
(13) Zhang, H.; Fonseca, A. F.; Cho, K., Tailoring Thermal Transport Property of Graphene through Oxygen Functionalization. *J. Phys. Chem. C* **2014,** *118*, 1436-1442.
(14) Wang, Z.; Xie, R.; Bui, C. T.; Liu, D.; Ni, X.; Li, B.; Thong, J. T. L., Thermal Transport in Suspended and Supported Few-Layer Graphene. *Nano Lett.* **2010,** *11*, 113-118.
(15) Jiang, J.-W.; Lan, J.; Wang, J.-S.; Li, B., Isotopic Effects on the Thermal Conductivity of Graphene Nanoribbons: Localization Mechanism. *J. Appl. Phys.* **2010,** *107*, 054314.
(16) Brito, W.; Kagimura, R.; Miwa, R., B and N Doping in Graphene Ruled by Grain Boundary Defects. *Phys. Rev. B* **2012,** *85*, 035404.
(17) Klemens, P.; Pedraza, D., Thermal Conductivity of Graphite in the Basal Plane. *Carbon* **1994,** *32*, 735-741.
(18) Xie, G.; Shen, Y.; Wei, X.; Yang, L.; Xiao, H.; Zhong, J.; Zhang, G., A Bond-Order Theory on the Phonon Scattering by Vacancies in Two-Dimensional Materials. *Scientific reports* **2014,** *4*.

(19) Ng, T.; Yeo, J.; Liu, Z., A Molecular Dynamics Study of the Thermal Conductivity of Graphene Nanoribbons Containing Dispersed Stone–Thrower–Wales Defects. *Carbon* **2012,** *50*, 4887-4893.
(20) Li, C.; Li, G.; Zhao, H., Hydrogenation Induced Deformation Mode and Thermal Conductivity Variations in Graphene Sheets. *Carbon* **2014,** *72*, 185-191.
(21) Kim, J. Y.; Lee, J.-H.; Grossman, J. C., Thermal Transport in Functionalized Graphene. *ACS Nano* **2012,** *6*, 9050-9057.
(22) Huang, W.; Pei, Q.-X.; Liu, Z.; Zhang, Y.-W., Thermal Conductivity of Fluorinated Graphene: A Non-Equilibrium Molecular Dynamics Study. *Chem. Phys. Lett.* **2012,** *552*, 97-101.
(23) Liu, Y.; Yang, H.; Liao, N.; Yang, P., Investigation on Thermal Conductivity of Bilayer Graphene Nanoribbons. *RSC Advances* **2014,** *4*, 54474-54479.
(24) Nika, D. L.; Cocemasov, A. I.; Balandin, A. A., Specific Heat of Twisted Bilayer Graphene: Engineering Phonons by Atomic Plane Rotations. *Appl. Phys. Lett.* **2014,** *105*, 031904.
(25) Peng, B.; Locascio, M.; Zapol, P.; Li, S.; Mielke, S. L.; Schatz, G. C.; Espinosa, H. D., Measurements of near-Ultimate Strength for Multiwalled Carbon Nanotubes and Irradiation-Induced Crosslinking Improvements. *Nat. Nanotechnol.* **2008,** *3*, 626-631.
(26) Kanasaki, J.; Inami, E.; Tanimura, K.; Ohnishi, H.; Nasu, K., Formation of Sp^{3}-Bonded Carbon Nanostructures by Femtosecond Laser Excitation of Graphite. *Phys. Rev. Lett.* **2009,** *102*, 087402.
(27) Cruz-Silva, E.; Botello-Méndez, A. R.; Barnett, Z. M.; Jia, X.; Dresselhaus, M. S.; Terrones, H.; Terrones, M.; Sumpter, B. G.; Meunier, V., Controlling Edge Morphology in Graphene Layers Using Electron Irradiation: From Sharp Atomic Edges to Coalesced Layers Forming Loops. *Phys. Rev. Lett.* **2010,** *105*, 045501.
(28) Zhan, H. F.; Zhang, Y. Y.; Bell, J. M.; Zhang, B. C.; Gu, Y. T., Tailoring the Resonance of Bilayer Graphene Sheets by Interlayer Sp3 Bonds. *J. Phys. Chem. C* **2013,** *118*, 732-739.
(29) Zhang, Y. Y.; Wang, C. M.; Cheng, Y.; Xiang, Y., Mechanical Properties of Bilayer Graphene Sheets Coupled by Sp^3 Bonding. *Carbon* **2011,** *49*, 4511-4517.
(30) Plimpton, S., Fast Parallel Algorithms for Short-Range Molecular Dynamics. *J. Comput. Phys.* **1995,** *117*, 1-19.
(31) Muller-Plathe, F., A Simple Nonequilibrium Molecular Dynamics Method for Calculating the Thermal Conductivity. *J. Chem. Phys.* **1997,** *106*, 6082-6085.
(32) Telling, R. H.; Ewels, C. P.; Ahlam, A.; Heggie, M. I., Wigner Defects Bridge the Graphite Gap. *Nat. Mater.* **2003,** *2*, 333-337.
(33) Brenner, D. W.; Shenderova, O. A.; Harrison, J. A.; Stuart, S. J.; Ni, B.; Sinnott, S. B., A Second-Generation Reactive Empirical Bond Order (Rebo) Potential Energy Expression for Hydrocarbons. *J. Phys.: Condens. Matter* **2002,** *14*, 783.
(34) Hoover, W. G., Canonical Dynamics: Equilibrium Phase-Space Distributions. *Phys. Rev. A* **1985,** *31*, 1695-1697.
(35) Nosé, S., A Unified Formulation of the Constant Temperature Molecular Dynamics Methods. *J. Chem. Phys.* **1984,** *81*, 511.
(36) Rajabpour, A.; Vaez Allaei, S. M., Tuning Thermal Conductivity of Bilayer Graphene by Inter-Layer Sp3 Bonding: A Molecular Dynamics Study. *Appl. Phys. Lett.* **2012,** *101*, 053115.
(37) Liu, X.; Zhang, G.; Zhang, Y.-W., Thermal Conduction across Graphene Cross-Linkers. *J. Phys. Chem. C* **2014**.
(38) Dickey, J.; Paskin, A., Computer Simulation of the Lattice Dynamics of Solids. *Phys. Rev.* **1969,** *188*, 1407.
(39) Sun, C. Q.; Tay, B.; Zeng, X.; Li, S.; Chen, T.; Zhou, J.; Bai, H.; Jiang, E., Bond-Order–Bond-Length–Bond-Strength (Bond-Ols) Correlation Mechanism for the Shape-and-Size Dependence of a Nanosolid. *J. Phys.: Condens. Matter* **2002,** *14*, 7781.
(40) Nika, D. L.; Balandin, A. A., Two-Dimensional Phonon Transport in Graphene. *J. Phys.: Condens. Matter* **2012,** *24*, 233203.
(41) Gaier, J. R.; YoderVandenberg, Y.; Berkebile, S.; Stueben, H.; Balagadde, F., The Electrical and Thermal Conductivity of Woven Pristine and Intercalated Graphite Fiber–Polymer Composites. *Carbon* **2003,** *41*, 2187-2193.
(42) Chen, S.; Wu, Q.; Mishra, C.; Kang, J.; Zhang, H.; Cho, K.; Cai, W.; Balandin, A. A.; Ruoff, R. S., Thermal Conductivity of Isotopically Modified graphene. *Nat. Mater.* **2012,** *11*, 203-207.
(43) Abeles, B., Lattice Thermal Conductivity of Disordered Semiconductor Alloys at High Temperatures. *Phys. Rev.* **1963,** *131*, 1906-1911.

Table of Contents